

1 **Diel Redox Cycle of Manganese in the Surface Arctic Ocean**

2 **Y. Xiang\*, P. J. Lam, J. M. Lee**

3 Department of Ocean Sciences, University of California, Santa Cruz, CA 95064 USA

4 Corresponding author: Yang Xiang ([yaxiang@ucsc.edu](mailto:yaxiang@ucsc.edu))

5

6 **Key Points:**

7 • Particulate manganese oxidation states are more reduced in the day and more oxidized at  
8 night in the surface Arctic Ocean;

9 • The Mn diel cycle results from the conversion between dissolved Mn and particulate  
10 Mn(III/IV) oxides regulated by light;

11 • The length of night and intensity of light exposure are two main controls on the magnitude  
12 of particulate Mn average oxidation states.

13

14

15

16

17

18

19

20

21 **Abstract**

22 Knowledge of the chemical speciation of particulate manganese (pMn) is important for  
23 understanding the biogeochemical cycling of Mn and other particle-reactive elements. Here, we  
24 present the synchrotron-based X-ray spectroscopy-derived average oxidation state (AOS) of pMn  
25 in the surface Arctic Ocean collected during the U.S. GEOTRACES Arctic cruise (GN01) in 2015.  
26 We show that the pMn AOS is less than 2.4 when sampled during the day and more than ~3.0  
27 when sampled at night. We hypothesize that an active light-dependent redox cycle between  
28 dissolved Mn and particulate Mn(III/IV) exists during the day-night cycle in the surface Arctic  
29 Ocean, which occurs on the timescale of hours. The magnitude of observed pMn AOS is likely  
30 determined by the net effect of the length of the previous night and integrated light level before  
31 the end of pMn sampling.

32 **Plain Language Summary**

33 Manganese (Mn) exists in three oxidation states (II, III, and IV) in the ocean. The difference in  
34 oxidation states of Mn minerals leads to differences in their capacities to oxidize and sorb other  
35 elements, and thereby affects their role in marine redox and nutrient cycling. In this study, we  
36 measured the oxidation states of marine particulate Mn in the surface Arctic Ocean. Our results  
37 demonstrate a tight coupling between sunlight and particulate Mn oxidation states: more Mn(II)  
38 exists in the daytime, whereas more Mn(III/IV) exists during the night. The light-dark cycle is an  
39 important driver in the rapid transition between Mn(II) and Mn(III/IV).

40

41 **Keywords:** Manganese; Photoreduction; Oxidation; Arctic Ocean; Synchrotron X-ray  
42 fluorescence (XRF); GEOTRACES

43 **1 Introduction**

44 Manganese (Mn) is the 3<sup>rd</sup> most abundant transition metal in Earth's crust and exists in  
45 three oxidation states (II, III, IV) in the ocean. Mn is an essential element to life and used to  
46 catalyze the oxidation of water to O<sub>2</sub> in Photosystem II (Yano et al., 2006) by phytoplankton, and  
47 to detoxify cells from superoxide radicals via the antioxidant enzyme Mn superoxide dismutase  
48 (Peers & Price, 2004). Oxidation from dissolved Mn(II) to particulate Mn(III/IV) oxides is known  
49 to proceed through two sequential, one-electron reactions (Luther, 2005). The final oxidation  
50 product, Mn(III/IV) oxide, is a strong natural oxidant and is also known as the “scavenger of the  
51 sea” (Goldberg, 1954; Tebo et al., 2004). Although Mn is an important micronutrient for  
52 phytoplankton growth, dissolved Mn is often characterized by maximum concentrations at the  
53 surface ocean (van Hulst et al., 2017) due to photoreduction of Mn(III/IV) oxides (Sunda &  
54 Huntsman, 1987, 1994; Sunda et al., 1983) and is thus not typically limiting, except for in the  
55 Southern Ocean (Browning et al., 2021; Middag et al., 2013).

56 Recent GEOTRACES cruises have demonstrated that the Arctic Ocean is enriched in Mn  
57 because of riverine, sedimentary and hydrothermal sources (Charette et al., 2020; Colombo et al.,  
58 2020; Jensen et al., 2020; Middag et al., 2011; Xiang & Lam, 2020). The Mn concentration in the  
59 Western Arctic Ocean is characterized by surface maxima in the Polar Mixed Layer in the  
60 dissolved phase and distinct elevations at halocline depths in the particulate phase (Jensen et al.,  
61 2020; Xiang & Lam, 2020). Investigations of Mn cycling in the Arctic Ocean have generally  
62 focused on processes spanning timescales of several months to years during transport from shelves  
63 to central basins. However, a diel cycle in the concentrations of Mn, in both dissolved and  
64 particulate phases, has been observed in the coastal Northwest Atlantic Ocean (Oldham et al., 2020;  
65 Sunda & Huntsman, 1990).

66 Here, we use synchrotron-based X-ray absorption spectroscopy (XAS) to examine the  
67 chemical speciation of particulate Mn (pMn) and its relationship with light during the U.S.  
68 GEOTRACES Arctic cruise (GN01) in 2015. We take advantage of sampling times that spanned  
69 a range of light conditions and relatively constant hydrographic parameters throughout the Polar  
70 Mixed Layer to reconstruct a pseudo-diel cycle. This study is one of few that focuses on the  
71 oxidation state of pMn in the ocean (Hermans et al., 2019; Lee et al., 2021; Oldham et al., 2021),  
72 and the first one in the Arctic Ocean. Lee et al. (2021) showed that changes in pMn speciation in  
73 the near- vs. far-field 15°S East Pacific Rise hydrothermal plume were associated with differences  
74 in its scavenging affinity for other trace elements and isotopes. Therefore, insights gained in this  
75 work help us understand the diel cycling of Mn and potentially also of other pMn-associated  
76 elements (e.g., cobalt; Moffett & Ho, 1996) in the surface Arctic Ocean.

77

## 78 **2 Materials and Methods**

### 79 2.1 Marine particle sampling and chemical analysis

80 Marine particles were sampled using dual-flow McLane Research in-situ pumps (WTS-  
81 LV) during the GN01 cruise onboard the U.S. Coast Guard Cutter *Healy* between 9 August and  
82 11 October 2015 (Figure 1). The day-night cycle varied tremendously over the course of the cruise  
83 and the length of night ranges from 0 to ~14 hours (Table S1).

84 Particles (0.8-51  $\mu\text{m}$ ) were collected with paired 0.8  $\mu\text{m}$  pore-size polyethersulfone  
85 Supor™ filters that were downstream of a 51  $\mu\text{m}$  pore-size polyester pre-filter. Filtered samples  
86 were dried in a laminar flow bench at room temperature upon recovery and stored in closed bags

87 in the dark before analysis. Concentrations of pMn were measured by high-resolution inductively  
88 coupled mass spectrometry after total digestion (Xiang & Lam, 2020).

## 89 2.2 Synchrotron X-ray Absorption Spectroscopy (XAS) analysis

90 Surface samples collected at ~20 m depth from 13 stations and one sample within the shelf  
91 benthic nepheloid layer, were analyzed by bulk XAS at the Stanford Synchrotron Radiation  
92 Lightsource Beamline 11-2. Prior to exposure to the light source, a subsample of the original filter  
93 (usually 1/32 of the whole, equivalent to ~12.5 L of pumped seawater) was rolled into multiple  
94 layers to maximize the signal from dilute marine particle samples. The speciation of pMn was  
95 determined by X-ray Absorption Near Edge Structure (XANES) spectroscopy using a liquid  
96 nitrogen cryostat. Averaged spectra were background removed, normalized and deglitched using  
97 the SIXPACK software package (Webb, 2005). No obvious shifts of XANES peaks were observed  
98 within 10-20 scans in all samples analyzed, indicating no Mn photoreduction had taken place  
99 during analysis (Figure S1). To assess variations in the speciation of pMn in the surface Arctic, we  
100 calculated the average oxidation state (AOS) of pMn from linear combination fitting of sample  
101 XANES spectra in the energy range of 6520-6600 eV using three Mn mineral endmembers to  
102 represent three oxidation states (II, III, IV) of Mn (Text S1).

## 103 2.3 Environmental parameters

104 Environmental parameters that can affect Mn redox cycling such as pH, temperature,  
105 oxygen, and light levels (Kim et al., 2012; Sunda & Huntsman, 1994; Toyoda & Tebo, 2016; Von  
106 Langen et al., 1997) were measured on the Oceanographic Data Facility (ODF) CTD rosette during  
107 the cruise (Landing et al., 2017; Woosley et al., 2017). Photosynthetically available radiation  
108 (PAR; wavelength of 400-700 nm) data was collected by a QCP-2300-HP Biospherical PAR

109 sensor. Since shortwave radiation in the UV-A range (wavelength of 350-380 nm) is thought to  
110 contribute most to reduction of Mn(III/IV) oxides (Sunda & Huntsman, 1994), and since PAR data  
111 were collected on different casts than particle samples, the solar zenith angle (SZA), defined as the  
112 angle between the sun and the vertical plane, is used to estimate the light level in the surface ocean  
113 during particle sampling. The SZA is less than 90° when the sun is above the horizon (“daylight”),  
114 and greater than 90° when the sun is below the horizon (“night”). The SZA was calculated with  
115 the National Oceanic and Atmospheric Administration Earth Systems Research Laboratory Solar  
116 Position Calculator (<http://www.esrl.noaa.gov/gmd/grad/solcalc/calcdetails.html>) by inputting  
117 sampling coordinates and times.

118 PAR values from the ODF CTD are negatively correlated with their corresponding SZA at  
119 20 decibars during the daytime (SZA<90°), and they are relatively constant and small at night  
120 (SZA>90°) (Figure 2a). The relationship between PAR and SZA observed during the ODF CTD  
121 casts suggests that the magnitude of SZA is a good proxy for visible light levels at 20 m where  
122 surface particles were collected, and by extension, possibly for UV-A light as well, given their  
123 similar attenuation coefficients (Lee et al., 2013). To account for different weather conditions  
124 experienced during the particle sampling at each station, which partly lead to scatter in the  
125 relationship between PAR and SZA, we also use underway shortwave radiation (wavelength of  
126 ~0.3-3 μm) data measured using a pyranometer above the sea surface at the helicopter deck. Note  
127 that underway shortwave radiation data cannot account for variable light attenuation by either ice  
128 cover or particles in the water column.

129

130 **3 Results and Discussion**

## 131 3.1 Surface pMn speciation

132 The surface Arctic has median (range) pMn concentrations of 1.0 (0.1-18.7) nmol/L (Table  
133 S1). The XANES spectra of surface samples analyzed show a pronounced maximum x-ray  
134 absorption peak either at 6561 eV or 6551 eV (Figure 3) which indicates oxidized and reduced  
135 pMn, respectively. Oxidized pMn samples (Stations 48, 52, 60) also have a shoulder peak at 6551  
136 eV, reflecting the existence of reduced Mn.

137 Two distinct x-ray absorption peaks at 6552 and 6557.5 eV occur in the benthic nepheloid  
138 layer (BNL) sample (Figure S2). Similar XANES spectra have been observed in estuarine  
139 sediments in San Francisco Bay (Carroll et al., 2002) and Baltic Sea sediments (Lenz et al., 2014),  
140 potentially suggesting a detrital pool of Mn aluminosilicates. We used the BNL XANES as a likely  
141 aluminosilicate reference to fit all surface Arctic samples. Station 6 is the only surface station  
142 dominated by the putative Mn aluminosilicates, with the BNL fraction accounting for 68.1% of  
143 the XANES signal (Figure S2), suggesting strong sediment resuspension on the Chukchi Shelf. To  
144 compare the non-aluminosilicate fraction to other surface samples, the BNL fraction was removed  
145 from the bulk XANES spectrum.

146 The pMn AOS estimated from XANES spectra range from 2.00 to 3.17 (Figure 1 & Table  
147 S1). More samples (10 out of 13) were characterized by reduced pMn (AOS<2.9) than oxidized  
148 pMn. The most oxidized surface pMn (Station 60; AOS=3.17) was best fit when the Mn(IV)  
149 reference ( $\delta$ -Mn<sup>IV</sup>O<sub>2</sub>) was included in the fits (Figure S3). For context, a reasonable expected upper  
150 limit for pMn AOS might be the oxidized pMn AOS (3.65) found within the perpetually dark  
151 Pacific-derived halocline (Station 14) (Figure S4). Since the measured AOS is the average

152 oxidation state, it likely includes a mix of Mn(IV) oxides and other forms of pMn with lower  
153 oxidation state, such as the pMn(II) found in surface waters (section 3.3).

### 154 3.2 Effect of light on pMn speciation

155 We separate XANES spectra into four groups based on the light level experienced during  
156 the 4-hour in-situ sampling and the day-night cycle characterizing that station. The first group  
157 experienced full light during sampling, even if a day-night cycle was present at that station  
158 (Stations 6, 43, 57, and 66); pMn is generally reduced in this group, characterized by a maximum  
159 absorption peak at 6551 eV (Figure 3a). Samples from Stations 43 and 57 also show small peaks  
160 at 6561 eV, indicating some presence of oxidized Mn. The second group comprises all surface  
161 samples at stations experiencing 24-hour light (Stations 19-38); these spectra exhibit a steep  
162 absorption peak at 6551 eV, characteristic of reduced Mn (Figure 3b). A small peak at 6560 eV  
163 observed at Station 32 is associated with a high Mn(III) fraction of 19.1% and little Mn(IV) (Table  
164 S1). Station 32, characterized by the shortest transport time from the shelf (~6 months) among all  
165 surface stations (Kipp et al., 2018), may have received shelf-derived particulate Mn(III/IV) that  
166 was transported laterally. The third group of samples were collected in partial darkness and are  
167 characterized by reduced Mn (Station 61) or a mixture of reduced and oxidized Mn (Stations 48  
168 and 60) (Figure 3c). The fourth group, comprising only one sample (Station 52), was collected in  
169 complete darkness. Similar to the more oxidized samples at Stations 48 and 60, pMn at Station 52  
170 is characterized by a mixture of reduced and oxidized Mn (Figure 3d).

171 To further describe the relationship between pMn speciation and light, we plot the AOS of  
172 pMn against the SZA (Figure 2b). We find that pMn is more oxidized when samples were taken  
173 at night ( $SZA > 90^\circ$ ), whereas it is more reduced when sampled during the day ( $SZA < 90^\circ$ ). Other

174 environmental parameters, e.g., temperature, dissolved oxygen, and pH, that are known to  
175 influence Mn oxidation (Toyoda & Tebo, 2016; Von Langen et al., 1997) and reduction (Kim et  
176 al., 2012; Sunda & Huntsman, 1994) kinetics, do not have clear correlations with pMn AOS in the  
177 surface Arctic during our cruise (Figure S5). Therefore, light levels appear to be the first-order  
178 control for pMn AOS in the surface Western Arctic.

### 179 3.3 Different pMn phases in the surface Arctic

180 Diel variations in the redox cycling of Mn have been observed in the coastal Northwest  
181 Atlantic Ocean (Oldham et al., 2020; Sunda & Huntsman, 1990). Although our data were not  
182 conducted at a single location over a 24-hour period, we treat our dataset as a pseudo-diel study  
183 and hypothesize that the high pMn AOS in the dark reflects the oxidation of dissolved Mn into  
184 Mn(III/IV) oxides at night (Sunda & Huntsman, 1990), and reduced AOS in the light results from  
185 the light-dependent reduction of Mn(III/IV) oxides during the day (Sunda & Huntsman, 1988,  
186 1994; Sunda et al., 1983). Photo-enhanced Mn(II) oxidation in the light mediated by reactions with  
187 reactive oxygen species has been reported in other environments and laboratory settings (Hansel  
188 & Francis, 2006; Learman et al., 2011; Nico et al., 2002). The lower AOS that we observed during  
189 the day suggests that light-dependent reduction is more important than photo-enhanced oxidation  
190 in the surface Arctic.

191 Sunda and Huntsman (1990) found that it was the ascorbate reducible fraction of pMn, i.e.,  
192 Mn(III/IV) oxides, that exhibited a diel pattern, whereas the ascorbate-resistant pMn remained  
193 relatively constant throughout the sampling period. We assume the pMn(II) observed in the surface  
194 Arctic Ocean is analogous to the ascorbate-resistant fraction noted above. Particulate Mn(II)  
195 accounted for a median (range) of 86.2% (23.7-100.0%) of total pMn (Table S1).

196 Ascorbate-resistant pMn could include cellular Mn, adsorbed Mn, and/or Mn(II)-  
197 containing minerals. Cellular Mn would presumably be organically-bound, but none of the  
198 organically-bound Mn(II) spectra found in the literature (Mn(II)-citrate, Mn(II)-EDTA, Mn  
199 superoxide dismutase, or Mn(II)-siderophores) had absorption peaks as low as 6551 eV (Figure  
200 S6 & Table S2) (Blamey et al., 2018; Gunter et al., 2006; Harrington et al., 2012; Machado et al.,  
201 2019). Mn(II)-containing aluminosilicates are unlikely to be important components of ascorbate-  
202 resistant pMn in the surface Arctic, given low concentrations of lithogenic material in the surface  
203 (cf., Xiang & Lam, 2020). Of the four Mn(II) adsorption standards we tested, only Mn(II) adsorbed  
204 to particulate inorganic carbon (PIC) exhibited an absorption peak close to 6551 eV, although post-  
205 edge features were not matched (Figure S6). We previously observed an unknown pMn(II) mineral  
206 in a hydrothermal plume (Lee et al., 2021) that contained a similarly low absorption peak at ~6551  
207 eV, but like the PIC adsorption standard, also had different post edge features (Figure S7). While  
208 we cannot confirm the identity of the observed surface pMn(II), we assume it is in the form of a  
209 non-photoactive Mn(II)-containing mineral.

210 We envision a conceptual model with a base level of non-photoactive pMn(II) that remains  
211 relatively constant through the day and night. The dissolved Mn pool is in excess of pMn in the  
212 surface Arctic Ocean (Jensen et al., 2020). At night, oxidation of ambient dissolved Mn adds  
213 pMn(III/IV) to the pMn pool that sinks. The fraction of pMn(III/IV) that remains suspended in the  
214 euphotic zone is completely reduced (timescale of hours; Sunda & Huntsman, 1994) and returns  
215 to the dissolved Mn pool during daytime. The total pMn concentrations and fractions of  
216 Mn(III)+Mn(IV) for oxidized samples collected in the dark from Stations 52 and 60 are 1.1 nM  
217 and 64.0%, and 18.7 nM and 76.3%, respectively (Table S1). Assuming all particulate Mn(III/IV)  
218 is derived from nightly oxidation of dissolved Mn, we calculate that particulate Mn(III/IV)

219 concentrations are 0.7 nM at Station 52 and 14.3 nM at Station 60. For simplicity, if we further  
220 assume that oxidation starts at dusk and loss of pMn by sinking is small, net Mn oxidation rates  
221 can be estimated by dividing the concentration of oxidized Mn by the length of darkness  
222 experienced from dusk to the end of sampling at each station (Stations 52 and 60: 6.2 and 2.9 hrs,  
223 respectively). Our estimated net Mn oxidation rates at Stations 52 and 60 are 0.11 and 4.9 nM/h,  
224 respectively. The much slower apparent oxidation rate at basin Station 52 might be explained by  
225 colder temperatures in the basin ( $\sim -1.5$  °C) compared to 0 °C at Station 60 at the shelf/slope, lower  
226 dissolved Mn concentrations (Jensen et al., 2020), and/or by different microbial communities (e.g.,  
227 Lee et al., 2019) affecting the rates of oxidation. These average rates integrating over 6.2 and 2.9  
228 hours are probably lower than the maximum oxidation rate in the surface Arctic but are generally  
229 comparable with other reported microbially mediated Mn oxidation rates of 0.1-50 nM/h in marine  
230 environments (Clement et al., 2009; Dick et al., 2009; Sunda & Huntsman, 1990).

### 231 3.4 Examination of controls on AOS in the surface Arctic

232 To examine the controls on the magnitude of pMn AOS, we use the length of night from  
233 the SZA data to estimate the extent of oxidation, and calculate the integrated shortwave radiation  
234 from dawn to the end of particle sampling for each station to estimate the extent of light-dependent  
235 reduction (Table S1). We consider shelf/slope and basin stations separately, since they have very  
236 different temperatures (Figure S5), nutrient levels, and light attenuation.

237 Both the length of night and intensity of light exposure after dawn influence the measured  
238 pMn AOS at the time of sampling: a longer period of darkness results in higher AOS at dawn,  
239 whereas higher integrated shortwave radiation decreases AOS in the light (Figure 4). We assume  
240 that all basin and shelf/slope stations have net Mn oxidation rates the same as Stations 52 (0.11  
241 nM/h) and 60 (4.9 nM/h), respectively (see section 3.3), and estimate the pMn(III/IV) formed at

242 night by multiplying the length of night at each station by the Mn oxidation rates (Table S1). To  
243 estimate the upper bound of AOS at dawn (hereafter the AOS<sub>dawn</sub>), we use the measured pMn(II)  
244 at time of sampling and assume it is constant throughout the day-night cycle and the estimated  
245 pMn(III/IV) produced during nighttime oxidation as pMn(IV) to calculate AOS<sub>dawn</sub> (Figure 4b).

246 The similar measured AOS at Stations 57 (2.37) and 43 (2.34) belies the different processes  
247 at work at these two basin stations: Station 57 had a longer night and thus higher estimated  
248 AOS<sub>dawn</sub>, but it also had higher integrated shortwave radiation by the time of sampling ( $1.42 \times 10^6$   
249 vs.  $2.06 \times 10^5$  J/m<sup>2</sup>), which decreased the AOS greatly (Figure 4a). Station 48 has the highest  
250 measured AOS (3.11) as a result of the high estimated AOS<sub>dawn</sub> (3.65) and the lowest integrated  
251 shortwave radiation ( $1.44 \times 10^5$  J/m<sup>2</sup>). Fully ice-covered basin Stations 19-38 were sampled under  
252 24-hour light conditions. Despite the expected attenuation in shortwave radiation from ice-cover  
253 (e.g., Lund-Hansen et al., 2015), it appears that extended exposure to even attenuated light (>3000  
254 hours) inhibits oxidation and results in low measured AOS (median=2.10) (Figure 2b).

255 At relatively warm and nutrient-rich shelf stations, higher Mn dark oxidation rates lead to  
256 higher estimated AOS (~4) at dawn compared to cold and oligotrophic basin stations (Figure 4b).  
257 At Stations 6 and 66, a high magnitude of integrated shortwave radiation ( $9.21 \times 10^6$  and  $2.22 \times 10^6$   
258 J/m<sup>2</sup>, respectively) leads to low measured AOS at the time of sampling (2.03 and 2.11,  
259 respectively). It is puzzling, however, to observe low measured AOS (2.11) at Station 61, despite  
260 having a high estimated AOS<sub>dawn</sub> (3.88) and low integrated shortwave radiation ( $2.35 \times 10^5$  J/m<sup>2</sup>)  
261 (Figure 4a). Factors such as temperature and microbial communities may lead to higher light-  
262 dependent Mn reduction rates at the shelf stations compared to basin stations. Alternatively, given  
263 the high concentrations of humic substances in the Chukchi Sea (Hioki et al., 2014; Nakayama et  
264 al., 2011), it is possible that Mn oxidation at night was inhibited at shelf stations (6, 61, 66) due to

265 strong dissolved Mn(III)-ligand complexes (Oldham et al., 2021). However, the inhibition of Mn  
266 oxidation cannot be a universal phenomenon in the Chukchi Sea, since slope Station 60 has a high  
267 AOS.

268

#### 269 **4 Conclusions**

270 The observed relationship between the pMn AOS and SZA demonstrates the significance  
271 of light in the Mn redox cycling in the Western Arctic Ocean. Such a relationship could also exist  
272 in other regions globally, but similar synchrotron-based analyses are more challenging due to much  
273 lower pMn concentrations compared to the surface Arctic Ocean.

274 We estimated that the Mn oxidation rate at night in the surface oligotrophic Arctic basins  
275 during our cruise is  $\sim 0.1$  nM/h. Such rates of Mn oxidation take place even within the near-freezing  
276 ( $\sim -1.5$  °C) Polar Mixed Layer in late summer. This study serves as the first study to infer in-situ  
277 Mn oxidation at such cold temperatures. The oxidation of dissolved Mn(II) in the extended polar  
278 winter with no sunlight could serve as a significant seasonal Mn removal mechanism out of the  
279 surface layer. Assuming that the Mn oxidation rate remains at 0.1 nM/h in the Arctic winter when  
280 it is dark 24 hrs a day, and that riverine and benthic sources of dissolved Mn diminish in winter, it  
281 would only take  $\sim 50$  hours ( $\sim 2$  days) to oxidize the entire reservoir of dissolved Mn in the surface  
282 Western Arctic Ocean ( $\sim 5$  nM; Jensen et al., 2020) and then sink out of the Polar Mixed Layer. To  
283 our knowledge, no measurements of dissolved or particulate Mn exist in the Arctic winter to test  
284 this prediction. Some of these exported Mn oxides during the dark night from the surface could  
285 contribute to the ubiquitous layers of sedimentary Mn oxides during interglacial times in the  
286 central Arctic Ocean (Löwemark et al., 2014).

287 To date, rapid redox cycles of Mn during the day-night cycle have been observed in the  
288 Western Arctic Ocean (this study) and coastal North Atlantic Ocean (Oldham et al., 2020; Sunda  
289 & Huntsman, 1990). In contrast, Mn oxidation is absent in the surface Sargasso Sea throughout  
290 the day and night, whereas it is present in the dark subsurface (Sunda & Huntsman, 1988). Oldham  
291 et al. (2021) did not detect pMn(IV) formation in either sun-lit surface or dark subsurface waters  
292 in the Ross Sea. The conditions that govern the diel Mn redox cycle are not clear, but have  
293 important implications for availability of Mn and other pMn-associated micronutrients. Future  
294 work is needed to investigate the relative importance of light levels, Mn(III)-ligand complexes,  
295 microbial communities, and/or reactive oxygen species in controlling Mn redox cycling and its  
296 impacts on biogeochemical cycles of different particle-reactive elements.

297

## 298 **Acknowledgments, Samples, and Data**

299 This work was supported by the Chemical Oceanography program through the National Science  
300 Foundation under grant number NSFOCE-1535854 to P.J.L. This research was carried out at the  
301 Stanford Synchrotron Radiation Lightsource, supported by the U.S. Department of Energy, Office  
302 of Science, Office of Basic Energy Sciences under Contract No. DE-AC02-76SF00515. We would  
303 like to thank all scientists and crew on board the USCGC icebreaker *Healy* during the GN01 Arctic  
304 GEOTRACES cruise. We thank co-chief scientist William Landing from Florida State University  
305 for providing underway shortwave radiation data, and Susan Becker from the Oceanographic Data  
306 Facility (ODF) at Scripps Institution of Oceanography for providing photosynthetically available  
307 radiation data. The ODF hydrographic, PAR, and pH data are available on the Biological and  
308 Chemical Oceanography Data Management Office (BCO-DMO) ([https://www.bco-](https://www.bco-dmo.org/dataset/700817)  
309 [dmo.org/dataset/700817](https://www.bco-dmo.org/dataset/700817) and <https://www.bco-dmo.org/dataset/646825>). The conversion between

310 voltage and  $\mu\text{E}/\text{m}^2/\text{s}$  in PAR data is based on the calibration conducted before the cruise.  
311 Particulate Mn data collected by in-situ pumps in the GN01 cruise are available on the BCO-DMO  
312 (<https://www.bco-dmo.org/dataset/807340>). Many thanks to Ryan C. Davis for the support at the  
313 Beamline 11-2, Carl Lamborg and Colleen Hansel for insights in the discussion, Benjamin  
314 Twining for providing Mn quota data for discussion, Colleen Hansel for providing XANES  
315 reference spectra including  $\delta\text{-MnO}_2$  and feitknechtite, Jena E. Johnson for Mn silicates reference  
316 spectra, Peter Kopittke for Mn citrate and oxalate reference spectra, and Hudson Carvalho for Mn-  
317 EDTA reference spectra. Thanks to two anonymous reviewers whose comments helped to improve  
318 this manuscript.

319

## 320 **References**

- 321 Blamey, F. P. C., McKenna, B. A., Li, C., Cheng, M., Tang, C., Jiang, H., et al. (2018). Manganese  
322 distribution and speciation help to explain the effects of silicate and phosphate on manganese  
323 toxicity in four crop species. *New Phytologist*, 217(3), 1146-1160.  
324 <https://doi.org/10.1111/nph.14878>
- 325 Browning, T. J., Achterberg, E. P., Engel, A., & Mawji, E. (2021). Manganese co-limitation of  
326 phytoplankton growth and major nutrient drawdown in the Southern Ocean. *Nature*  
327 *Communications*, 12(1), 884. <https://doi.org/10.1038/s41467-021-21122-6>
- 328 Carroll, S., O'Day, P. A., Esser, B., & Randall, S. (2002). Speciation and fate of trace metals in  
329 estuarine sediments under reduced and oxidized conditions, Seaplane Lagoon, Alameda Naval  
330 Air Station (USA). *Geochemical Transactions*, 3(10), 81-101.  
331 <https://doi.org/10.1039/B205002A>
- 332 Charette, M. A., Kipp, L. E., Jensen, L. T., Dabrowski, J. S., Whitmore, L. M., Fitzsimmons, J. N.,  
333 et al. (2020). The Transpolar Drift as a source of riverine and shelf-derived trace elements to

334 the central Arctic Ocean. *Journal of Geophysical Research: Oceans*, 125(5).

335 <https://doi.org/10.1029/2019jc015920>

336 Clement, B. G., Luther, G. W., & Tebo, B. M. (2009). Rapid, oxygen-dependent microbial Mn(II)

337 oxidation kinetics at sub-micromolar oxygen concentrations in the Black Sea suboxic zone.

338 *Geochimica et Cosmochimica Acta*, 73(7), 1878-1889.

339 <https://doi.org/10.1016/j.gca.2008.12.023>

340 Colombo, M., Jackson, S. L., Cullen, J. T., & Orians, K. J. (2020). Dissolved iron and manganese

341 in the Canadian Arctic Ocean: On the biogeochemical processes controlling their distributions.

342 *Geochimica et Cosmochimica Acta*, 277, 150-174. <https://doi.org/10.1016/j.gca.2020.03.012>

343 Dick, G. J., Clement, B. G., Webb, S. M., Fodrie, F. J., Bargar, J. R., & Tebo, B. M. (2009).

344 Enzymatic microbial Mn(II) oxidation and Mn biooxide production in the Guaymas Basin

345 deep-sea hydrothermal plume. *Geochimica et Cosmochimica Acta*, 73(21), 6517-6530.

346 <https://doi.org/10.1016/j.gca.2009.07.039>

347 Goldberg, E. D. (1954). Marine Geochemistry 1. Chemical Scavengers of the Sea. *The Journal of*

348 *Geology*, 62(3), 249-265

349 Gunter, K. K., Aschner, M., Miller, L. M., Eliseev, R., Salter, J., Anderson, K., & Gunter, T. E.

350 (2006). Determining the oxidation states of manganese in NT2 cells and cultured astrocytes.

351 *Neurobiology of Aging*, 27(12), 1816-1826.

352 <https://doi.org/10.1016/j.neurobiolaging.2005.10.003>

353 Hansel, C. M., & Francis, C. A. (2006). Coupled photochemical and enzymatic Mn(II) oxidation

354 pathways of a planktonic *Roseobacter*-like bacterium. *Applied and Environmental*

355 *Microbiology*, 72(5), 3543. <https://doi.org/10.1128/AEM.72.5.3543-3549.2006>

- 356 Harrington, J. M., Parker, D. L., Bargar, J. R., Jarzecki, A. A., Tebo, B. M., Sposito, G., &  
357 Duckworth, O. W. (2012). Structural dependence of Mn complexation by siderophores: Donor  
358 group dependence on complex stability and reactivity. *Geochimica et Cosmochimica Acta*, 88,  
359 106-119. <https://doi.org/10.1016/j.gca.2012.04.006>
- 360 Hermans, M., Lenstra, W. K., van Helmond, N. A. G. M., Behrends, T., Egger, M., Séguret, M. J.  
361 M., et al. (2019). Impact of natural re-oxygenation on the sediment dynamics of manganese,  
362 iron and phosphorus in a euxinic Baltic Sea basin. *Geochimica et Cosmochimica Acta*, 246,  
363 174-196. <https://doi.org/10.1016/j.gca.2018.11.033>
- 364 Hioki, N., Kuma, K., Morita, Y., Sasayama, R., Ooki, A., Kondo, Y., et al. (2014). Laterally  
365 spreading iron, humic-like dissolved organic matter and nutrients in cold, dense subsurface  
366 water of the Arctic Ocean. *Scientific Reports*, 4, 6775. <https://doi.org/10.1038/srep06775>
- 367 Jensen, L. T., Morton, P. L., Twining, B. S., Heller, M. I., Hatta, M., Measures, C. I., et al. (2020).  
368 A comparison of marine Fe and Mn cycling: U.S. GEOTRACES GN01 Western Arctic case  
369 study. *Geochimica et Cosmochimica Acta*, 288, 138-160.  
370 <https://doi.org/10.1016/j.gca.2020.08.006>
- 371 Kim, K., Yoon, H. I., & Choi, W. (2012). Enhanced dissolution of manganese oxide in ice  
372 compared to aqueous phase under illuminated and dark conditions. *Environmental Science &*  
373 *Technology*, 46(24), 13160-13166. <https://doi.org/10.1021/es302003z>
- 374 Kipp, L. E., Charette, M. A., Moore, W. S., Henderson, P. B., & Rigor, I. G. (2018). Increased  
375 fluxes of shelf-derived materials to the central Arctic Ocean. *Science advances*, 4(1),  
376 eaao1302. <https://doi.org/10.1126/sciadv.aao1302>
- 377 Landing, W. M., Cutter, G., & Kadko, D. C. (2017). CTD-ODF profiles from GEOTRACES-  
378 Arctic Section cruise HLY1502, August to October 2015 (U.S. GEOTRACES Arctic project).

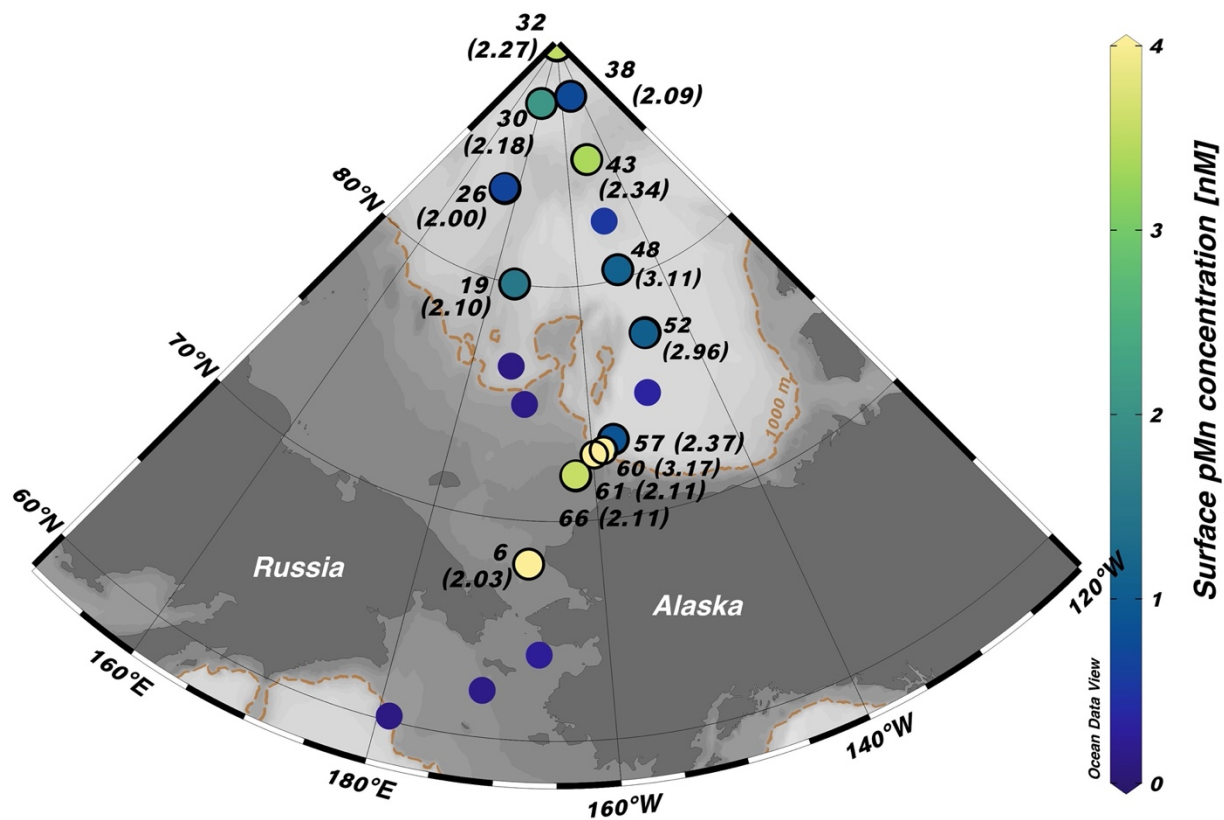
- 379 *Biological and Chemical Oceanography Data Management Office (BCO-DMO), Dataset*  
380 *version 2017-05-22*. Retrieved from <http://lod.bco-dmo.org/id/dataset/700817>
- 381 Learman, D. R., Wankel, S. D., Webb, S. M., Martinez, N., Madden, A. S., & Hansel, C. M. (2011).  
382 Coupled biotic–abiotic Mn(II) oxidation pathway mediates the formation and structural  
383 evolution of biogenic Mn oxides. *Geochimica et Cosmochimica Acta*, 75(20), 6048-6063.  
384 <https://doi.org/10.1016/j.gca.2011.07.026>
- 385 Lee, J., Kang, S. H., Yang, E. J., Macdonald, A. M., Joo, H. M., Park, J., et al. (2019). Latitudinal  
386 distributions and controls of bacterial community composition during the summer of 2017 in  
387 Western Arctic Surface waters (from the Bering Strait to the Chukchi Borderland). *Scientific*  
388 *Reports*, 9(1), 16822. <https://doi.org/10.1038/s41598-019-53427-4>
- 389 Lee, J. M., Lam, P. J., Vivancos, S. M., Pavia, F. J., Anderson, R. F., Lu, Y., et al. (2021). Changing  
390 chemistry of particulate manganese in the near- and far-field hydrothermal plumes from 15°S  
391 East Pacific Rise and its influence on metal scavenging. *Geochimica et Cosmochimica Acta*,  
392 300, 95-118. <https://doi.org/10.1016/j.gca.2021.02.020>
- 393 Lee, Z., Hu, C., Shang, S., Du, K., Lewis, M., Arnone, R., & Brewin, R. (2013). Penetration of  
394 UV-visible solar radiation in the global oceans: Insights from ocean color remote sensing.  
395 *Journal of Geophysical Research: Oceans*, 118(9), 4241-4255.  
396 <https://doi.org/10.1002/jgrc.20308>
- 397 Lenz, C., Behrends, T., Jilbert, T., Silveira, M., & Slomp, C. P. (2014). Redox-dependent changes  
398 in manganese speciation in Baltic Sea sediments from the Holocene Thermal Maximum: An  
399 EXAFS, XANES and LA-ICP-MS study. *Chemical Geology*, 370, 49-57.  
400 <https://doi.org/10.1016/j.chemgeo.2014.01.013>

- 401 Löwemark, L., März, C., O'Regan, M., & Gyllencreutz, R. (2014). Arctic Ocean Mn-stratigraphy:  
402 genesis, synthesis and inter-basin correlation. *Quaternary Science Reviews*, 92, 97-111.  
403 <https://doi.org/10.1016/j.quascirev.2013.11.018>
- 404 Lund-Hansen, L. C., Markager, S., Hancke, K., Stratmann, T., Rysgaard, S., Ramløv, H., & Sorrell,  
405 B. K. (2015). Effects of sea-ice light attenuation and CDOM absorption in the water below  
406 the Eurasian sector of central Arctic Ocean (>88°N). *Polar Research*, 34(0).  
407 <https://doi.org/10.3402/polar.v34.23978>
- 408 Luther, G. W. (2005). Manganese(II) oxidation and Mn(IV) reduction in the environment—two  
409 one-electron transfer steps versus a single two-electron step. *Geomicrobiology Journal*, 22(3-  
410 4), 195-203. <https://doi.org/10.1080/01490450590946022>
- 411 Machado, B. A., Gomes, M. H. F., Marques, J. P. R., Otto, R., & de Carvalho, H. W. P. (2019).  
412 X-ray spectroscopy fostering the understanding of foliar uptake and transport of Mn by  
413 soybean (*Glycine max* L. Merrill): Kinetics, chemical speciation, and effects of glyphosate.  
414 *Journal of Agricultural and Food Chemistry*, 67(47), 13010-13020.  
415 <https://doi.org/10.1021/acs.jafc.9b05630>
- 416 Middag, R., de Baar, H. J. W., Klunder, M. B., & Laan, P. (2013). Fluxes of dissolved aluminum  
417 and manganese to the Weddell Sea and indications for manganese co-limitation. *Limnology  
418 and Oceanography*, 58(1), 287-300. <https://doi.org/10.4319/lo.2013.58.1.0287>
- 419 Middag, R., de Baar, H. J. W., Laan, P., & Klunder, M. B. (2011). Fluvial and hydrothermal input  
420 of manganese into the Arctic Ocean. *Geochimica et Cosmochimica Acta*, 75(9), 2393-2408.  
421 <https://doi.org/10.1016/j.gca.2011.02.011>

- 422 Moffett, J. W., & Ho, J. (1996). Oxidation of cobalt and manganese in seawater via a common  
423 microbially catalyzed pathway. *Geochimica et Cosmochimica Acta*, 60(18), 3415-3424.  
424 [https://doi.org/10.1016/0016-7037\(96\)00176-7](https://doi.org/10.1016/0016-7037(96)00176-7)
- 425 Nakayama, Y., Fujita, S., Kuma, K., & Shimada, K. (2011). Iron and humic-type fluorescent  
426 dissolved organic matter in the Chukchi Sea and Canada Basin of the western Arctic Ocean.  
427 *Journal of Geophysical Research: Oceans*, 116(C7). <https://doi.org/10.1029/2010jc006779>
- 428 Newville, M. (2001). IFEFFIT: Interactive XAFS analysis and FEFF fitting. *Journal of*  
429 *Synchrotron Radiation*, 8(2), 322-324. <https://doi.org/10.1107/S0909049500016964>
- 430 Nico, P. S., Anastasio, C., & Zamoski, R. J. (2002). Rapid photo-oxidation of Mn(II) mediated by  
431 humic substances. *Geochimica et Cosmochimica Acta*, 66(23), 4047-4056.  
432 [https://doi.org/10.1016/S0016-7037\(02\)01001-3](https://doi.org/10.1016/S0016-7037(02)01001-3)
- 433 Oldham, V. E., Chmiel, R., Hansel, C. M., DiTullio, G. R., Rao, D., & Saito, M. A. (2021).  
434 Inhibited manganese oxide formation hinders cobalt scavenging in the Ross Sea. *Global*  
435 *Biogeochemical Cycles*, n/a(n/a), e2020GB006706. <https://doi.org/10.1029/2020GB006706>
- 436 Oldham, V. E., Lamborg, C. H., & Hansel, C. M. (2020). The spatial and temporal variability of  
437 Mn speciation in the coastal Northwest Atlantic Ocean. *Journal of Geophysical Research:*  
438 *Oceans*, 125(1), e2019JC015167. <https://doi.org/10.1029/2019JC015167>
- 439 Peers, G., & Price, N. M. (2004). A role for manganese in superoxide dismutases and growth of  
440 iron-deficient diatoms. *Limnology and Oceanography*, 49(5), 1774-1783.  
441 <https://doi.org/10.4319/lo.2004.49.5.1774>
- 442 Sunda, W. G., & Huntsman, S. A. (1987). Microbial oxidation of manganese in a North Carolina  
443 estuary1. *Limnology and Oceanography*, 32(3), 552-564.  
444 <https://doi.org/10.4319/lo.1987.32.3.0552>

- 445 Sunda, W. G., & Huntsman, S. A. (1988). Effect of sunlight on redox cycles of manganese in the  
446 southwestern Sargasso Sea. *Deep Sea Research Part A. Oceanographic Research Papers*,  
447 35(8), 1297-1317. [https://doi.org/10.1016/0198-0149\(88\)90084-2](https://doi.org/10.1016/0198-0149(88)90084-2)
- 448 Sunda, W. G., & Huntsman, S. A. (1990). Diel cycles in microbial manganese oxidation and  
449 manganese redox speciation in coastal waters of the Bahama Islands. *Limnology and*  
450 *Oceanography*, 35(2), 325-338. <https://doi.org/10.4319/lo.1990.35.2.0325>
- 451 Sunda, W. G., & Huntsman, S. A. (1994). Photoreduction of manganese oxides in seawater *Marine*  
452 *Chemistry*, 46, 133-152. [https://doi.org/10.1016/0304-4203\(94\)90051-5](https://doi.org/10.1016/0304-4203(94)90051-5)
- 453 Sunda, W. G., Huntsman, S. A., & Harvey, G. R. (1983). Photoreduction of manganese oxides in  
454 seawater and its geochemical and biological implications. *Nature*, 301(5897), 234.  
455 <https://doi.org/10.1038/301234a0>
- 456 Tebo, B. M., Bargar, J. R., Clement, B. G., Dick, G. J., Murray, K. J., Parker, D., et al. (2004).  
457 Biogenic manganese oxides: Properties and mechanisms of formation. *Annual Review of*  
458 *Earth and Planetary Sciences*, 32(1), 287-328.  
459 <https://doi.org/10.1146/annurev.earth.32.101802.120213>
- 460 Toyoda, K., & Tebo, B. M. (2016). Kinetics of Mn(II) oxidation by spores of the marine *Bacillus*  
461 sp. SG-1. *Geochimica et Cosmochimica Acta*, 189, 58-69.  
462 <https://doi.org/10.1016/j.gca.2016.05.036>
- 463 van Hulst, M., Middag, R., Dutay, J. C., de Baar, H., Roy-Barman, M., Gehlen, M., et al. (2017).  
464 Manganese in the west Atlantic Ocean in the context of the first global ocean circulation model  
465 of manganese. *Biogeosciences*, 14(5), 1123-1152. <https://doi.org/10.5194/bg-14-1123-2017>

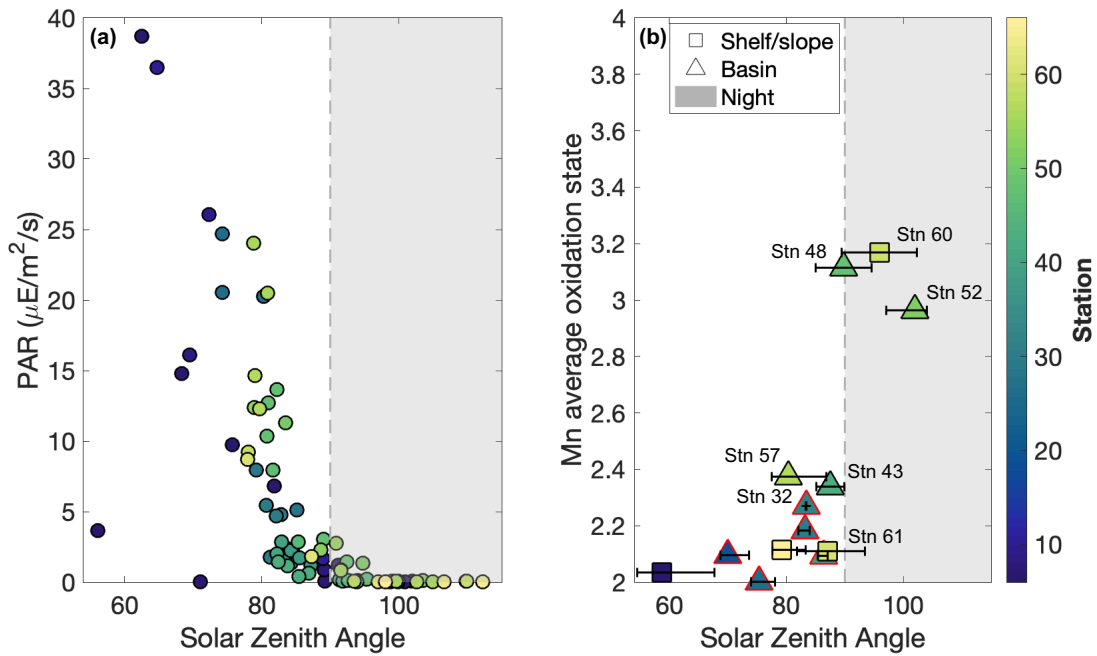
- 466 Von Langen, P. J., Johnson, K. S., Coale, K. H., & Elrod, V. A. (1997). Oxidation kinetics of  
467 manganese (II) in seawater at nanomolar concentrations. *Geochimica et Cosmochimica Acta*,  
468 61(23), 4945-4954. [https://doi.org/10.1016/S0016-7037\(97\)00355-4](https://doi.org/10.1016/S0016-7037(97)00355-4)
- 469 Webb, S. M. (2005). SIXPack a graphical user interface for XAS analysis using IFEFFIT. *Physica*  
470 *Scripta*, 1011. <https://doi.org/10.1238/physica.topical.115a01011>
- 471 Woosley, R. J., Millero, F. J., & Takahashi, T. (2017). Internal consistency of the inorganic carbon  
472 system in the Arctic Ocean. *Limnology and Oceanography: Methods*, 15(10), 887-896.  
473 <https://doi.org/10.1002/lom3.10208>
- 474 Xiang, Y., & Lam, P. J. (2020). Size-fractionated compositions of marine suspended particles in  
475 the Western Arctic Ocean: Lateral and vertical sources. *Journal of Geophysical Research:*  
476 *Oceans*, 125(8), e2020JC016144. <https://doi.org/10.1029/2020JC016144>
- 477 Yano, J., Kern, J., Sauer, K., Latimer, M. J., Pushkar, Y., Biesiadka, J., et al. (2006). Where water  
478 is oxidized to dioxygen: Structure of the photosynthetic Mn4Ca cluster. *Science*, 314(5800),  
479 821-825. <https://doi.org/10.1126/science.1128186>
- 480
- 481
- 482
- 483
- 484
- 485
- 486
- 487



488

489 **Figure 1.** Sampling locations of the GN01 cruise (cruise track: clockwise). Colors show the  
 490 surface particulate Mn (pMn) concentrations (unit: nmol/L). Average oxidation states (AOS) of  
 491 pMn analyzed by XANES are labeled next to station numbers within parenthesis.

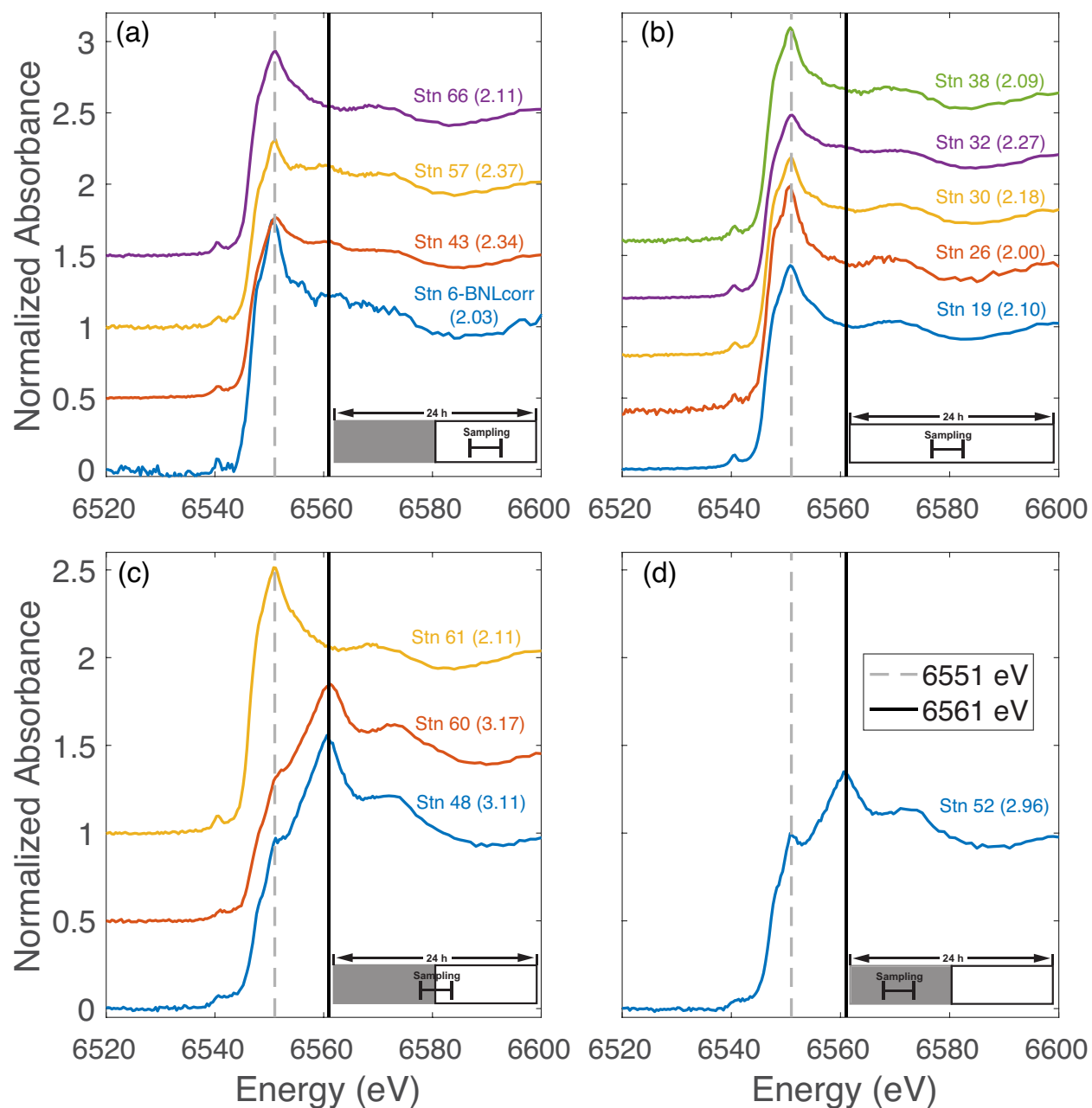
492



493

494 **Figure 2.** The relationships between SZA and PAR measured in the ODF CTD casts at pressure=  
 495 20 decibars (a), and between SZA and Mn AOS measured on particles collected in the pump casts  
 496 at ~20 m (b). The symbols in (b) are the SZA at mid-cast and error bars demonstrate the minimum  
 497 and maximum SZA during particle sampling. Samples collected under 24-h light conditions are  
 498 outlined in red.

499

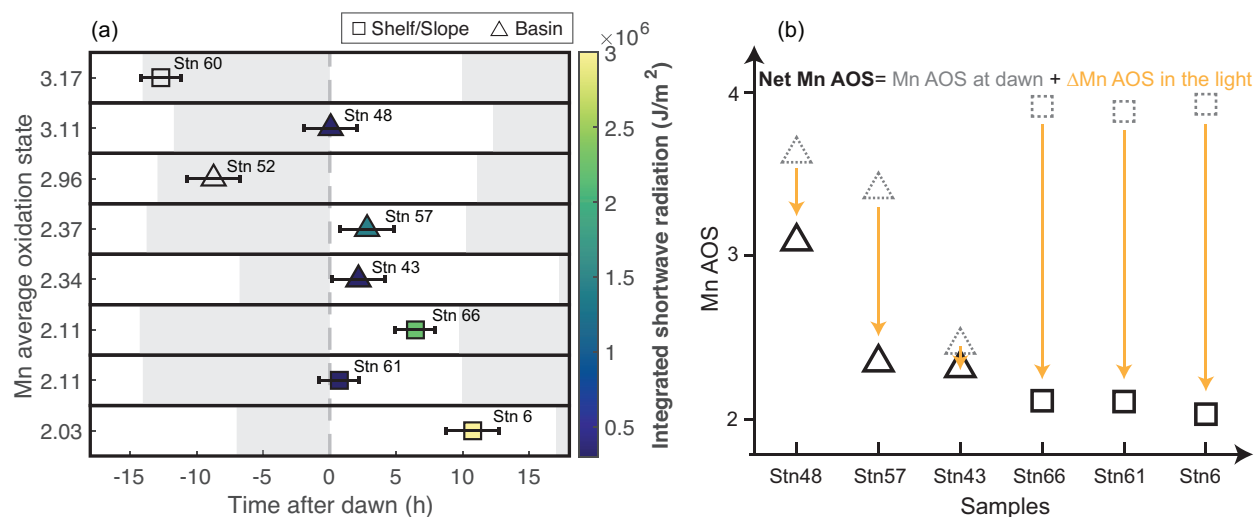


500

501 **Figure 3.** Mn K-edge bulk XANES spectra of surface pMn analyzed, grouped by different light  
 502 levels experienced during the sampling and/or on a daily basis. The selection criteria for four  
 503 groups are displayed as a cartoon in the bottom right corner of each subplot, illustrating whether  
 504 there was a day-night cycle at that station during sampling (white-shaded rectangle) and the light  
 505 level during sampling (horizontal bar). (a): sampling entirely in the light but experiencing a day-

506 night cycle; (b): sampling entirely in the light and experiencing 24-h light; (c): sampling partially  
 507 in the light; (d): sampling entirely in the dark but experiencing a day-night cycle. The pMn AOS  
 508 for each spectrum is labeled within parenthesis.

509



510

511 **Figure 4.** The relationship between time after dawn (unit: hour) and pMn AOS (a), and a schematic  
 512 diagram of AOS during the day-night cycle (b). Shelf/slope and basin stations are marked as  
 513 squares and triangles respectively. In panel (a), the length of night is indicated by the shaded  
 514 rectangle for each station and the color bar is the integrated shortwave radiation (unit: J/m<sup>2</sup>) from  
 515 dawn to the end of particle sampling. Error bars demonstrate the period of in-situ particle sampling  
 516 in the water column, typically 3-4 hours. The black solid symbols in (b) are the net pMn AOS  
 517 measured by XANES, whereas grey dashed symbols are estimated AOS maxima at dawn  
 518 (AOS<sub>dawn</sub>) calculated based on the length of night and Mn oxidation rates.

519